The stability of bcc-Fe at high pressures and temperatures with respect to tetragonal strain

Lidunka Vočadlo, Ian G. Wood, Michael J. Gillan, John Brodholt, David P. Dobson, G. David Price, Dario Alfè

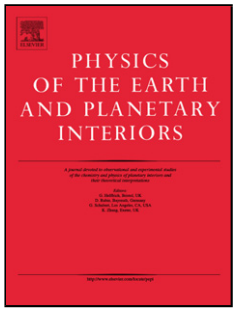

Title: The stability of bcc-Fe at high pressures and temperatures with respect to tetragonal strain

Authors: Lidunka Vočadlo, Ian G. Wood, Michael J. Gillan, John Brodholt, David P. Dobson, G. David Price, Dario Alfè

PII: S0031-9201(08)00187-8
DOI: doi:10.1016/j.pepi.2008.07.032
Reference: PEPI 5018

To appear in: *Physics of the Earth and Planetary Interiors*

Received date: 11-10-2007
Revised date: 19-6-2008
Accepted date: 18-7-2008

Please cite this article as: Vočadlo, L., Wood, I.G., Gillan, M.J., Brodholt, J., Dobson, D.P., Price, G.D., Alfè, D., The stability of bcc-Fe at high pressures and temperatures with respect to tetragonal strain, *Physics of the Earth and Planetary Interiors* (2007), doi:10.1016/j.pepi.2008.07.032

The stability of bcc-Fe at high pressures and temperatures with respect to tetragonal strain

Lidunka Vočadlo[a,d], Ian G Wood[a], Michael J Gillan[b,d], John Brodholt[a,d], David P Dobson[a], G.David Price[a,d] and Dario Alfè[a,b,c,d]

[a] Department of Earth Sciences, University College London, Gower Street, London WC1E 6BT, UK.

[b] Department of Physics and Astronomy, University College London, Gower Street, London WC1E 6BT, UK.

[c]London Centre for Nanotechnology, 17-19 Gordon Street, London WC1H 0AH

[d] Materials Simulation Laboratory, University College London, Gower Street, London WC1E 6BT, UK.

Abstract

The phase that iron adopts at the conditions of the Earth's inner core is still unknown. The two primary candidates are the hexagonal-close-packed (hcp) structure and the body-centred-cubic (bcc) structure polymorphs. Until recently, the former was favoured, but it now seems possible that bcc iron could be present. A remaining uncertainty regarding the latter phase is whether or not bcc iron is stable with respect to tetragonal strain under core conditions. In this paper, therefore, we present the results of high precision ab initio free energy calculations at core pressures and temperatures performed on bcc iron as a function of tetragonal strain. Within the uncertainties of the calculations, direct comparison of free energy values suggests that bcc may be unstable with respect to tetragonal strain at 5500 K; this is confirmed when the associated stresses are taken into account. However, at 6000 K, the results indicate that the bcc phase becomes more stable, although it is unclear as to whether complete stability has been achieved. Nevertheless, it remains distinctly possible that the addition of light elements could stabilise this structure convincingly. Therefore, bcc-Fe cannot be ruled out as a candidate inner core phase.

Introduction

The exact composition of the Earth's inner core is not very well known. On the basis of cosmochemical and geochemical arguments, it has been suggested that the core is an iron alloy with possibly as much as ~5 wt.% Ni and very small amounts (only fractions of a wt% to trace) of other siderophile elements such as Cr, Mn, P and Co (McDonough and Sun, 1995). On the basis of materials-density/sound-wave velocity systematics, Birch (1964) further concluded that the iron must be alloyed with a small fraction (2 - 4 wt.%) of lighter elements. The light alloying elements most commonly suggested include S, O, Si, H and C, although minor amounts of other elements, such K, could also be present (e.g. Poirier, 1994; Gessmann and Wood, 2002, Alfè et al., 2002).

The properties of the inner core are determined by the composition and structure of the materials that are present, and, therefore ideally we would like to know the thermoelastic properties of iron alloyed with light elements over the full range of pressure and temperature conditions experienced by the Earth's core. However even the behaviour of pure iron is poorly understood. Experimentalists have put an enormous effort over the last

15-20 years into obtaining a phase diagram of pure iron, but above relatively modest pressures and temperatures there is still much uncertainty (Brown 2001). Under ambient conditions, Fe adopts a body centred cubic (bcc) structure that transforms with temperature to a face centred cubic (fcc) form (at ~ 1200 K), and with pressure transforms to a hexagonal close packed (hcp) phase (at ~10-15 GPa). At higher pressures and temperatures, however, the phase diagram of pure iron is especially controversial (see Fig 1). Diamond-anvil cell (DAC) studies have been interpreted as showing that hcp Fe transforms at high temperatures to a phase which has variously been described as having a double hexagonal close packed structure (dhcp) (Saxena et al., 1996) or an orthorhombically distorted hcp structure (Andrault et al., 1997). Furthermore, high pressure shock experiments have also been interpreted as showing a high pressure solid-solid phase transformation (Brown and McQueen, 1986; Brown, 2001). It has been suggested that this transition could be due to the development of a bcc phase (Ross et al., 1990; Matsui and Anderson, 1997). Other experimentalists, however, have failed to detect such a post-hcp phase (e.g. Shen et al., 1998; Nguyen and Holmes, 2004), and have suggested that the previous observations were due either to minor impurities or to metastable strain-induced behaviour. Figure 1 also shows that there is also considerable disagreement between different theoretical studies. However, until recently, the general consensus in theoretical calculations has been that the stable phase of iron in the Earth's core is likely to be the hcp phase (Stixrude et al., 1997; Vočadlo et al., 2000) and that it was only the melting curve that was in dispute.

The bcc phase of iron was considered an unlikely candidate as a core-forming phase for three main reasons: (i) it is elastically unstable at high pressures and 0 K, (ii) it is vibrationally unstable at high pressures and 0 K, and (iii) it is thermodynamically unstable at high pressures and temperatures with respect to the hexagonal-close-packed (hcp) phase (Vočadlo et al., 2003). The evidence for these statements is summarised below, together with a discussion of the various possible phase transitions that might be found in iron at high pressures and temperatures.

The elastic instability of the bcc phase at 0 K is well known from theoretical calculations (Söderlind et al., 1996; Stixrude et al., 1994; Strixrude and Cohen, 1995; Vočadlo et al., 1997). At ambient conditions, the bcc phase (c/a = 1) is the stable form of iron, but at high pressures elastic distortions of the cubic cell by compression along [001] result in a local minimum at c/a = 0.87-0.88 (sometimes referred to as body-centred-tetragonal or bct) at ~150 GPa that with further distortion is unstable relative to the fcc phase. Alternatively, compression along the [110] direction to ~180 GPa results in a spontaneous direct distortion to the fcc structure (equivalent to a tetragonal strain with c/a = $\sqrt{2}$). It should be noted that the transformation to the thermodynamically more stable hcp phase at 10-15 GPa is a reconstructive transition and so does not occur spontaneously during such simulations.

The vibrational instabilities of high-pressure bcc iron have also been studied before (Söderlind et al., 1996; Strixrude and Cohen, 1995; Vočadlo et al., 2000; Vočadlo et al., 2003), but because of their key role in this work, we show in Fig 2 our results for the phonon dispersion relations as a function of pressure. The frequencies have been recast from the results of Vočadlo et al (2003) to show their behaviour around the N-point in the at the Brillioun zone boundary. It can be seen that the onset of the instability of bcc-Fe at high pressure occurs below ~180 GPa where one of the branches in the N [½ ½ 0] direction becomes unstable first at the zone centre, Γ, (associated with the $bcc \rightarrow fcc$ transition) and then at the N-point (associated with the $bcc \rightarrow hcp$ martensitic transition). There is also a

third instability occurring below ~260 GPa, along the [111] direction (Γ to H); the pattern of the displacement involved in this instability involves the relative movement of planes of atoms in the [111] direction of the cubic cell. It is this pattern of displacement that is directly involved in the bcc to omega (ω) phase transition (see below). The transition behaviour to the *hcp* and *ω* phases is very similar to that observed in Group IV metals in the bcc phase (Petry et al., 1991); however, it is interesting to note that Hf, Zr abd Ti do not display an initial zone centre instability to the *fcc* phase, but rather, as has been observed, transform first to the ω phase (Sikka et al., 1982).

We have previously shown that the hcp and fcc phases are vibrationally stable at high pressures (Vočadlo et al., 2000) and in Fig. 3 we show the phonon dispersion relations for the ω phase of iron as a function of pressure. It can be seen that the ω phase is also vibrationally stable as a function of pressure above 0 GPa, and remains so to pressures far in excess of those in the Earth's interior. Note, however, that this phase becomes vibrationally unstable at negative pressures with the frequencies of several of the phonon branches becoming imaginary (not shown).

As already mentioned, this bcc to ω transition is known to readily occur in other transition metals (Petry, 1995; Trampenau et al., 1991; Grad et al., 2000) and may easily be understood by recognising that both the bcc and ω phases can be represented using a dimensionally hexagonal unit cell, where the c axis of the hexagonal setting is equivalent to the [111] direction of the cubic bcc cell. Both structures have three atoms in the unit cell and have similar c/a ratios ($\sqrt{3/8}$). The fractional atomic coordinates of these two phases are then given by:

		ω			*bcc*	
atom 1	0	0	0	0	0	0
atom 2	1/3	2/3	1/2	1/3	2/3	1/3
atom 3	2/3	1/3	1/2	2/3	1/3	2/3

These two structures are shown in Fig 4, together with that of the face-centred-cubic (fcc) phase, which can also be represented using a hexagonal cell. It is clear that the transformation between the bcc and ω phases occurs via small displacements of atoms 2 and 3 above in the c direction (equivalent to the [111] direction of the cubic bcc cell), and it is, therefore, not surprising that a spontaneous distortion from the bcc to the ω phase might occur. It is worth noting that changing the c/a ratio of the bcc setting above to $\sqrt{6}$ produces the fcc phase.

Despite the mechanical stability of the various phases described above, our calculations show that, at 0 K, the relative enthalpies of the bcc, ω, fcc phases with respect to the hcp phase at V=7.2 Å/atom (~260 GPa) are 1.845, 0.765 and 0.256 eV/atom respectively, confirming that the hcp phase is the thermodynamically most stable phase at high pressure (and 0 K), as expected. However, when the effect of temperature is included using ab initio molecular dynamics calculations, Vočadlo et al. (2003) presented results that indicated that the bcc phase becomes dynamically stable and energetically more stable than the ω phase above ~3500 K (Figs 5 and 6).

The paper by Vočadlo et al. (2003) also addressed the thermodynamic stability of the bcc phase of iron at core conditions. It was shown that the calculated free energy of bcc-Fe at V=7.2 Å/atom and 5500 K is only marginally higher than that for hcp (by ~35 meV). The assumption that iron must have the hcp structure at core conditions, especially in the presence of lighter elements, had already been challenged (Beghein and Trampert, 2003; Lin et al., 2002; Ishii and Dziewonski, 2002), and so Vočadlo et al. (2003) presented calculations that suggested that a small amount of light element impurity could indeed stabilise the bcc phase at the expense of the hcp phase in the Earth's inner core (see also Côté et al., 2007). We note that nickel, by contrast, crystallises in the fcc structure and stabilises fcc Fe–Ni alloys relative to pure Fe (e.g., Lin et al., 2002; Mao et al., 2006). Therefore the fcc phase cannot necessarily be ruled out as a candidate inner core phase, despite being thermodynamically less stable than the hcp phase at core conditions.

The evidence presented by Vočadlo et al. (2003) for the mechanical stability of bcc-Fe at core conditions included discussion of the hydrostatic nature of the stresses on the simulation box (Fig. 5). It could, however, be argued that these stresses did not necessarily correspond to a free energy minimum, but might instead be at a local maximum with the unit cell metastable with respect to a finite tetragonal strain. Therefore, in an attempt to resolve this issue of the stability of bcc-Fe, we present in this paper ab initio free energy calculations of the bcc phase as a function of tetragonal strain.

Computational method

The calculations presented are based on Density Functional Theory (DFT) (Hohenberg and Kohn, 1964) within the Generalised Gradient Approximation (Wang and Perdew, 1991) implemented in the code VASP (Kresse and Furthmüller, 1996), with the Projected Augmented Wave method (Blöchl, 1994, Kresse and Joubert, 1999) used to describe the electronic interactions with the atomic nuclei, and with an efficient extrapolation of the electronic charge density which halves the simulation time (Alfè, 1999). In first principles molecular dynamics, the ions are treated as classical particles and, for each set of atomic positions, the electronic energy is solved within the framework of DFT which includes the thermal excitations of the electrons. The calculations were performed without spin polarisation as we have already shown that there is no magnetic moment at the pressures and temperatures of the inner core (Vočadlo et al., 2003).

The stability of bcc-Fe was determined with respect to strain by calculating the free energy of a system with a volume of 7.2 $Å^3$/atom and a temperature of 5500 K (equivalent to ~290 GPa). The calculations were performed at different values of c/a ranging from 0.85 to 1.5, thereby including the previously reported spontaneous transitions to fcc (at c/a=√2) and the local minimum at c/a ~ 0.87-0.88. Full details of the methodology can be found in Vočadlo and Alfè (2002) and Alfè et al. (2002).

The free energy of the bcc solid, F_{bcc}, may be given by the sum of two contributions, that of the perfect non-vibrating crystal, $F_{perfect}$, and that due to the atomic motions above 0 K, $F_{vibrational}$, thus:

$$F_{bcc} = F_{perfect} + F_{vibrational} \quad (1)$$

Where the vibrational free energy has a harmonic and anharmonic component respectively:

$$F_{vibrational} = F_{harmonic} + F_{anharmonic} \quad (2)$$

When calculating the free energy of the bcc crystal in this way, we have a problem: the bcc phase is vibrationally unstable at high pressures and zero K so the harmonic contribution to the free energy is not tractable. Furthermore, in calculating the anharmonic contribution, for materials which are vibrationally stable, an appropriate reference system would be the harmonic crystal. One way around this is to calculate the free energy of the bcc system using thermodynamic integration from some other reference system. In principle we could use as the reference system a simple inverse power potential that we have previously shown to work well for iron at Earth's core conditions, including liquid Fe, hcp- and bcc-Fe (Alfè et al., 2001, 2002; Vočadlo et al., 2003) and which is given by:

$$U_{IP} = 4\varepsilon\left(\frac{\Gamma}{r}\right)^{\alpha} \quad (3)$$

Where ε = 1eV, Γ = 1.77Å and α = 5.86. However, for c/a < 1, this reference system also becomes vibrationally unstable with imaginary frequencies appearing in the phonon spectrum. It is important to stress here that the choice of the reference system does not affect the final answer for *F*, although it does affect the efficiency of the calculations. Therefore, to address the issue of this simple inverse-power reference system being unstable for c/a<1, it is perfectly valid to add a potential U_E which stabilises the crystal. We chose to use an Einstein model, with the potential U_E given by:

$$U_E = \sum_{i=1}^{n} \frac{1}{2} k u_i^{\,2} \quad (4)$$

where $u_i = | r_i - r_i^0 |$ represents the displacement of atom i from its perfect crystal position r_i^0 and k is a constant. The total "pseudo-harmonic" potential now acting on the atoms is therefore given by $U_{pseudo\_harm} = U_{harm} + U_E$, where U_{harm} is the original harmonic component of the inverse power potential. The effect of this stratagem is shown in the resulting phonon (Fig. 7). This approach produces a "pseudo-harmonic" vibrational spectrum with real frequencies throughout the range of c/a studied, allowing the calculation of the harmonic contribution to the free energy.

At this stage, we note, however, that the reference system which best matches the ab initio system (and therefore minimises the time taken to do the calculations) may be achieved through a linear combination of the pseudoharmonic system (to maintain vibrational stability, 10%), $U_{pseudo\text{-}harm,}$ and the inverse power potential (90%), U_{IP}:

$$U_{ref} = 0.1U_{pseudo-harm} + 0.9U_{IP} \quad (5)$$

The free energy of this mixed reference system is then found in two stages by: (i) calculating the free energy of the pseudo-harmonic system and (ii) thermodynamically integrating between this and the mixed reference system.

For a given temperature, T, the free energy per atom of the pseudo-harmonic system is given by:

$$F_{pseudo-harm} = 3k_B T \ln(\beta\hbar\bar{\omega}) \quad (6)$$

Where k_B is Boltzmann's constant, ħ is Planck's constant/2π, $\beta=1/k_BT$ and $\bar{\omega}$ is the geometric average of the phonon frequencies, which is defined by:

$$\ln\bar{\omega} = \frac{1}{N_q N_i}\sum_{q,i}\ln(\omega_{qi}) \quad (7)$$

Where $\omega_{q,i}$ are the phonon frequencies of branch *i* and wave vector *q*, N_i is the total number of phonon branches and N_q is the number of q-points in the sum. The phonon frequencies are calculated using the PHON code (Alfè, 1998) which implements the small displacement method (for details see Kresse et at., 1996; Alfè et al., 2001; Vočadlo and Alfè, 2002).

The free energy of the reference system, F_{ref} (90% IP and 10% pseudo-harmonic), may then be calculated using thermodynamic integration from the pseudo-harmonic system:

$$F_{ref} = F_{pseudo-harm} + \int_0^1 d\lambda \left\langle U_{ref} - U_{pseudo-harm} \right\rangle_\lambda \quad (8)$$

where U_{ref} and $U_{pseudo\text{-}harm}$ are the potential energies of the pseudo-harmonic and reference system respectively, and $\langle . \rangle_\lambda$ is the thermal average in the ensemble generated by $U_\lambda = \lambda U_{ref} + (1-\lambda)U_{pseudo\text{-}harm}$.

Alternatively, we can adopt the dynamical method described by Watanabe and Reinhardt (1990). In this approach the parameter λ depends on time and is slowly (adiabatically) switched from 0 to 1 during a single simulation. The switching rate has to be slow enough so that the system remains in thermodynamic equilibrium and adiabatically transforms from the pseudo-harmonic to the reference system. The change in free energy is then given by:

$$\Delta F = \int_0^{t_{total}} dt \frac{d\lambda}{dt}\left(U_{ref} - U_{pseudo-harm}\right) \quad (9)$$

where t_{total} is the total simulation time, $\lambda(t)$ is an arbitrary function of t with the property of being continuous and differentiable for $0<t<1$, $\lambda(0)=0$, and $\lambda(t_{total})=1$.

When using this second method, it is important to ensure that the switching is adiabatic, i.e., that t_{total} is sufficiently large. One possible way to test this is to change λ from 0 to 1 in the first half of the simulation and then from 1 back to 0 in the second half of the simulation, evaluating ΔF in each case; the average of the two values is then taken as the best estimate for ΔF, and the difference is a measure of the non-adiabaticity, and also, of course, of the statistical error. If this difference is less than the desired uncertainty, one can be confident that the simulation time is sufficiently long. In our calculations we chose a total simulation time of sufficient length such that the difference in ΔF between the two calculations was less than one meV/atom.

The free energy of the reference system was calculated in this way on a 1000 atom (10x10x10 supercell of the primitive cell) box with a volume of 7.2 Å^3/atom over a range of c/a ratios between 0.85 and 1.5; these calculations involve only the classical potentials U_{IP} and $U_{pseudo\text{-}harm}$, so they could be run for 100 ps, which ensured convergence of the free energy difference F_{ref}-$F_{pseudo\text{-}harm}$ to less than 1 meV/atom.

Once the free energy of the reference system was obtained, thermodynamic integration was then used again to calculate the full free energy of the ab initio system at each c/a. However, as these are ab intio calculations it is not practical to use Eq. 9 above. Instead we use the small-lambda approximation of Eq. 8 (Alfè et al., 2002):

$$F - F_{ref} \cong \left\langle U - U_{ref} \right\rangle_{ref} - \frac{1}{2k_B T}\left\langle \left[U - U_{ref} - \left\langle U - U_{ref} \right\rangle_{ref} \right]^2 \right\rangle_{ref} \quad (10)$$

where, in this case, U is potential energy of the ab initio system, and F is free energy of the ab initio system. This approximation is only justified if the fluctuations in U-U_{ref} are small (which can be achieved by the use of a suitably accurate reference potential); indeed, if the fluctuations are small, with the second term in the right-hand-side of Eq. 10 contributing only a few meV/atom, Eq. 10 can be truncated and becomes:

$$F - F_{ref} \cong \left\langle U - U_{ref} \right\rangle_{ref} \quad (11)$$

This is a particularly useful form of Eq. 8 as one needs only to sample the phase space of the reference system and to perform only a relatively small number of static *ab initio* calculations on statistically independent configurations extracted from the long classical simulations (typically 40 configurations extracted from a 20 ps classical run). For this study, the calculations were performed on 128 atom (4x4x4 supercell of the cubic 2-atom box) cell with a 2x2x2 k-point grid, equivalent to 4 k-points in the irreducible wedge of the Brilloiun zone.

Results

Having dealt at length with the current evidence for the stability of the various phases of iron over a range of pressures and temperatures, and having described the detailed technicalities of the computational method necessary in the present work, our results may be presented very concisely. Our calculated free energy as a function of tetragonal strain for a volume of 7.2 Å^3/atom (~290 GPa) and a temperature of 5500 K is shown in Fig. 8. The free energies calculated from the reference system using Eq. 9 are shown together with three points calculated using the full expression for thermodynamic integration (Eq. 8) integrating between $\lambda = 0$ and $\lambda = 1$. The uncertainties in the free energies range from a few meV to ~10 meV per atom, although most are between 5 and 10 meV per atom. Despite the cluster of points around c/a = 1, the associated uncertainties make it difficult to resolve categorically whether bcc is locally stable in this region directly from this figure, although, at first glance, instability seems more likely.

The matter could, in principle, be resolved by examination of the stresses on the simulation box as a function of c/a. For bcc to be stable, the quantity $(\sigma_x + \sigma_y)/2 - \sigma_z$ should be negative

for c/a<1 and positive for c/a>1. Figure 9 shows this stress difference as a function of c/a at a zero-strain volume of 7.05 $Å^3$/atom for three systems: a supercell of 64 atoms at 5500 K, a supercell of 128 atoms at 5500 K and a supercell of 64 atoms at 6000 K. Within the uncertainties, the result is converged in supercell size at 5500 K and suggests instability in the bcc structure. Indeed, this result is consistent with Fig. 8: the energy required to pull the cell from c/a=0.96 to bcc (c/a=1) is, from Fig. 9, the product of the stress difference and the distance of the distortion – i.e., for a 2-atom cell, ~2 x 10^9 x 0.04 x 14.4 x 10^{-30}/(1.602 x 10^{-19}) = ~ 7 meV. This is approximately the value suggested by inspection of Fig. 8. However at 6000 K, this instability is significantly reduced to the extent that $(\sigma_x + \sigma_y)/2 - \sigma_z$ is invariant close to c/a = 1 and therefore, even with very long simulation times to reduce the uncertainties as much as possible (50-70 ps), neither stability nor instability can be demonstrated, although the structure is clearly very close to being stable.

Conclusions

Previous calculations on different phases of iron (Vočadlo et al., 2003) suggested that the bcc phase becomes entropically stabilised by temperature at core pressures. However, these calculations did not take into account the possibility of bcc-Fe being unstable with respect to tetragonal strain (i.e., not at a local minimum in the free energy surface). Despite the enormous efforts that went into reducing our uncertainties as much as possible, our free energy calculations as a function of tetragonal strain in the present study do not allow us to resolve this issue irrefutably. However when an analysis of the stresses on the simulation box is made, the results show that the bcc phase is, in fact, unstable with respect to tetragonal strain at 5500 K, but becomes significantly more stable at 6000 K. While it is difficult to say whether stability has actually been achieved due to the invariance of the stress difference close to c/a = 1, clearly temperature serves to appreciably increase the stability of the bcc phase at core conditions.

We already know that for *pure* iron, the hcp phase is still found to have marginally the lowest free energy (Vočadlo et al., 2003) and is, therefore, the thermodynamically more stable phase under core conditions. However, the difference in free energy between hcp- and bcc-Fe is very small (~35 meV). It is becoming increasingly recognised that the effect of incorporation of light elements could stabilise the bcc phase over the hcp phase in the inner core; indeed, this effect has already been shown experimentally at lower pressures (Lin et al., 2002). It has also been shown that iron alloyed with nickel at very high pressures and temperatures (>225 GPa, <3400 K) adopts the bcc structure (Dubrovinsky et al., 2007). It is, therefore, distinctly possible that light elements and/or nickel could stabilise the bcc phase with respect to tetragonal strain. This is particularly important given the evidence for a seismically distinct region in the upper part of the inner core which might be explained by such a body-centred alloy. The presence of bcc iron would have important consequences for interpretation of the elastic properties of the inner core which are currently based on the assumption that the hcp phase is the only stable structure of iron under core conditions.

Acknowledgements: LV, DPB and DA would like to thank the Royal Society for their support; DA also acknowledges support from EPSRC through the EURYI award. LV would also like to thank Alex Côté for help in the preparation of the manuscript. Finally LV would like to thank Lars Stixrude for initiating this highly lengthy and detailed study and then taking the time to read and comment on the finished product!

REFERENCES

Ahrens T J, Holland K G and Chen C Q 2002 Phase diagram of iron, revised core temperatures *Geophys. Res.Lett.* **29** 1150

Alfè, D 1999 Ab-initio molecular dynamics, a simple algorithm for charge extrapolation *Comp. Phys. Comm.*, **118**, 31-33

Alfè, D 1998 Program available at http://chianti.geol.ucl.ac.uk/~dario

Alfè, D, Price, G D and Gillan, M J 2001 Thermodynamics of hexagonal close packed iron under Earth's core conditions *Phys. Rev. B*, **64,** 045123 1-16

Alfè, D, Price, G D and Gillan, M J 2002 Iron under Earth's core conditions: liquid-state thermodynamics and high pressure melting curve from *ab initio* calculations. *Phys. Rev. B* **65**, 165118-1-11.

Alfè, D, Price, G D and Gillan, M J 2002 Ab-initio chemical potentials of solid and liquid solutions and the chemistry of the Earth's core. *J. Chem. Phys.*, **116,** 7127-7136.

Andrault D, Fiquet G, Kunz M, Visocekas F, Hausermann D 1997 The orthorhombic structure of iron: and in situ study at high temperature and high pressure. *Science* **278**, 831-834

Andrault D, Fiquet G, Charpin T and Le Bihan T 2000 Structure analysis and stability field f iron at high pessure and temperature *Am. Mineral.* **85** 364–71

Beghein C, Trampert J 2003 Robust normal mode constraints on inner core anisotropy from model space search. *Science* **299**, 552-555

Belonoshko AB, Ahuja R, Johansson B 2000 Quasi-ab initio molecular dynamics study of Fe melting. *Phys. Rev. Lett.* **84**, 3638-3641.

Birch F 1964 Density and composition of the mantle and core. *J. Geophys. Res.* **69**, 4377-4388

Blöchl, P E Projector augmented-wave method. 1994 *Phys. Rev. B* **50**, 17953-17979

Boehler R 1993 Temperatures in the Earth's core from melting point measurements of iron at high static pressures. *Nature* **363**, 534-536

Brown JM 2001 The equation of state of iron to 450 GPa: another high pressure phase? *Geophys. Res. Lett*. **28**, 4339-4342

Brown JM, McQueen RG 1986 Phase transitions, Grüneisen parameter and elasticity of shocked iron between 77 GPa abd 400 GPa. *J. Geophys. Res.* **91**, 7485-7494

Côté AS, Vočadlo L, Brodholt J 2006 The effect of silicon impurities on the phase diagram of iron and possible implications for the Earth's core structure. *Under submission.*

Dubrovinsky L et al., 2007 Body-centred cubic iron-nickel alloy in Earth's core. *Science*, **316**, 1880-1883

Dziewonski AM, Anderson, DL 1981 Preliminary reference Earth model. *Phys. Earth Planet. Int.* **25**, 297-356

Gessmann CK, Wood BJ 2002 Potassium in the Earth's core? *Earth Planet.Sci. Lett.* **200**, 63-78

Grad 2000 Grad, G. B. et al. Electronic structure and chemical bonding effects upon the bcc to phase transition: *ab initio* study of Y, Zr, Nb and Mo. *Phys. Rev. B*, **62**, 12,743-12,753

Hohenberg, P and Kohn, W 1964 Inhomogeneous electron gas. *Phys. Rev.* **136**, B864-871

Ishii M and Dziewonski AM 2002 The innermost inner core of the Earth: evidence for a change in anisotropic behaviour at a radius of about 300 km. *Proc. Nat. Acad. Sci.* **99**, 14,026-14,030

Kresse, G and Furthmüller, J 1996 Efficient iterative schemes for *ab initio* total-energy calculations using a plane-wave basis set *Phys. Rev. B* **54**, 11169-11186

Kresse G, Furthmüller, J and Hafner J 1995 Ab initio force constant approach to phonon dispersion relations of diamond and graphite *Europhys. Lett.* **32**, 729-734

Kresse, G and Joubert D 1999 From ultrasoft pseudopotentials to the projected augmented-wave method. *Phys. Rev. B* **59** 1758-1775

Laio A, Bernard S, Chiarotti G L, Scandolo S and Tosatti E 2000 Physics of iron at earth's core conditions *Science* **287** 1027

Lin JF, Heinz DL, Campbell AJ, Devine, JM, Shen GY 2002 Iron-silicon alloy in the Earth's core? *Science* **295**, 313-315

Lin JF, Heinz DL, Campbell AJ, Devine JM, Mao WL and Shen GY 2002 Iron–nickel alloy in the Earth's core. *Geophys. Res. Lett.* **29** art. no. 1471

Matsui M, Anderson OL 1997 The case for a body-centred cubic phase (alpha ') for iron at inner core conditions. *Phys. Earth Planet. Int.* **103,** 55-62

Mao W, Campbell AJ, Heinz DL and Shen G 2006 Phase relations of Fe–Ni alloys at high pressure and temperature. *Earth Planet. Sci. Lett.* **155** 146–151

McDonough WF, Sun S-s 1995 The composition of the Earth. *Chem. Geol.* **120**, 223-253

Nguyen JH, Holmes NC 2004 Melting of iron at the physical conditions of the Earth's core. *Nature* **427**, 339-342

Petry, W 1995 Dynamical precursors of martensitic transitions. *J. de Phys. IV* **5**, C2-15-C2-28

Pertry, W et al., Phonon dispersion of the bcc phase of Group IV metals I: bcc titanium. *Phys. Rev. B* **43**, 10,933-10,947

Poirier JP 1994 Light elements in the Earth's outer core: a critical review. *Phys. Earth Planet. Int.* **85**, 319-337

Ross M, Young DA, Grover R 1990 Theory of the iron phase diagram at Earth's core conditions. *J. Geophys. Res*., **95**, 21713-21716

Saxena SK, Dubrovinsky LS 2000 Iron phases at high pressures and temperatures: phase transitions and melting. *Amer. Mineral.* **85**, 372-375

Saxena SK, Dubrovinsky LS, Haggkvist P 1996 X-ray evidence for the new phase of beta-iron at high temperature and high pressure. *Geophys. Res. Lett*. **23**, 2441-2444

Shen GY, Mao HK, Hemley RJ, Duffy TS, Rivers ML 1998 Melting and crystal structure of iron at high pressures and temperatures. *Geophys. Res. Lett.* **25**, 373-376.

Shen GY, Prakapenka VB, Rivers ML, Sutton SL 2004 Structure of liquid iron at pressures up to 58 GPa. Phys. Rev. Lett. 92, #185701

Sikka SK, Vohra YK, Chidambaram R 1982 Omega phase in materials *Prog. Mat. Sci.,* **27** 245-310

Söderlind P, Moriarty JA, Wills JM 1996 First principles theory of iron up to earth's core pressures: structural, vibrational and elastic properties. *Phys. Rev. B* **53**, 14063-14072

Stixrude L, Cohen, RE and Singh, DJ 1994 Iron at high pressure: linearised augmented plane wave calculations in the generalised gradient approximation. *Phys. Rev. B* **50**, 6442-6445

Stixrude L, Cohen RE 1995 Constraints on the crystalline structure of the inner core – mechanical stability of bcc iron at high pressure. *Geophys. Res. Lett.* **22**, 125-128

Stixrude L, Wasserman E, Cohen RE 1997 Composition and temperature of the Earth's inner core. *J. Geophys. Res*. **102**, 24729-24739

Trampenau J, Heiming A, Petry W, Alba M, Herzig C, Miekeley W and Schober HR 1991 Phonon dispersion of the bcc phase of group-IV metals. III. bcc hafnium. *Phys. Rev. B* **43** 10963-10969

Vočadlo L, de Wijs G, Kresse G, Gillan MJ, Price GD 1997 First Principles Calculations on Crystalline and Liquid Iron at Earth's Core Conditions. *Faraday Discussions* **106**: 'Solid-State Chemistry - New Opportunities from Computer Simulations' 205-217.

Vočadlo L 2006 Ab initio calculations of the elasticity of iron and iron alloys at inner core conditions: evidence for a partially molten inner core. *EPSL in press.*

Vočadlo L, Dobson DP, Wood IG 2006 Ab initio study of nickel substitution into iron. *Earth Plan. Sci. Lett.* In press.

Vočadlo L, Alfe D 2002 Ab initio melting curve of the fcc phase of aluminium. *Phys. Rev. B* **65**, 214105:1-12

Vočadlo L, Alfe D, Gillan MJ, Wood IG, Brodholt JP, Price GD 2003a Possible thermal and chemical stabilisation of body-centred-cubic iron in the Earth's core. *Nature* **424**, 536-539

Vočadlo L**,** Alfe D, Gillan MJ, Price GD 2003b The properties of iron under core conditions from first principles calculations. *Phys. Earth Planet. Int.*, **140**, 101-125.

Vočadlo L, Brodholt JP, Alfe D, Gillan MJ, Price GD 2000 Ab initio free energy calculations on the polymorphs of iron at core conditions. *Phys. Earth Planet. Int.* **117**, 123-137

Wallace, DC 1998 *Thermodynamics of Crystals* Dover Publications, New York

Wang, Y. & Perdew, J. 1991 Correlation hole of the spin-polarized electron gas, with exact small-wave-vector and high-density scaling. *Phys. Rev. B* **44**, 13298-13307.

Watanabe M and Reinhardt WP 1990 Direct dynamical calculation of entropy and free energy by adiabatic switching. Phys. Rev. Lett. **65**, 3301-3304

Williams Q, Jeanloz R, Bass J D, Svendesen B and Ahrens T J 1987 The melting curve of iron to 250gigapascals—a constraint on the temperature at the Earth's center *Science* **236** 181–2

Yoo C S, Holmes N C, Ross M, Webb D J and Pike C 1993 Shock temperatures and melting of iron at Earth core conditions *Phys. Rev. Lett.* **70** 3931–4

Figure Captions

Figure 1: Phase diagram of pure iron. Solid lines represent phase boundaries and melt lines from DAC experiments; symbols with error bars are points on the melting curve from shock experiments; broken lines are melting curves from first-principles calculations. DAC data: Ref a: Saxena and Dubrovinsky, 2000; b: Andrault et al., 2000; c: Shen et al., 1998; d: Williams et al., 1987; e: Boehler, 1993. Shock data: triangle: Yoo et al., 1993; circles: Brown and McQueen, 1986; reverse triangle: Ahrens et al., 2002; diamond: Nguyen and Holmes, 2004. First principles calculations; f: Laio et al., 2000; g: Alfè et al., 2002; h: Vočadlo et al., 2000 (where the arrow indicates stability is maintained to high temperature); i: Vočadlo et al., 2003. Adapted from Nguyen and Holmes, 2004.

Figure 2: Phonon dispersion relations in bcc iron at 0 K as a function of pressure. The onset of the instability of *bcc*-Fe occurs below ~180 GPa in the [½ ½ 0] direction associated with the $bcc \rightarrow fcc$ transition at the zone centre, and the $bcc \rightarrow hcp$ transition at the N-point (imaginary frequencies are represented here as negative values). A second instability occurs below 260 GPa in the [111] direction associated with the $bcc \rightarrow \omega$ transition. Calculations on the *bcc* structure in the hexagonal setting at 0 K and at a fixed volume of 7.2 $Å^3$ per atom (~260 GPa) show that the *bcc* phase spontaneously distorts to the ω phase; however, it must be noted that the enthalpy of the ω phase is 0.77 eV/atom higher than the *hcp*-phase at these conditions, confirming that the *hcp*-Fe is the thermodynamically stable phase at high pressure and 0K, as expected.

Figure 3: Phonon dispersion relations for the omega phase. It can be seen that this phase is vibrationally stable to pressures well beyond that of the inner core; however, it is not thermodynamically stable with respect to the hcp phase, this latter phase being the stable phase at high pressures and zero Kelvin.

Figure 4: The structure of the a) bcc, b) fcc and c) ω phases of iron in the hexagonal setting. The bcc and ω phases have the same c/a ratio and differ only in the heights of the atoms. The pale dotted lines indicate the conventional bcc and fcc unit cells with orthogonal axes as marked.

Figure 5: The calculated stress tensors (upper row) and atomic position correlation functions (lower row) for a 64 atom cubic supercell of bcc iron as a function of simulation time and temperature. The structure deviates from the *bcc* phase below 3000K (from Vočadlo et al., 2003).

Figure 6: Structure factors for the perfect *bcc* and ω phases compared with those from the MD simulations on a 135 atom supercell as a function of temperature. Note that the peaks unique to the ω phase at ~6 $Å^{-1}$, ~7 $Å^{-1}$ and ~8.7 $Å^{-1}$ grow with decreasing temperature (from Vočadlo et al., 2003).

Figure 7: Vibrational spectrum of bcc Fe at V=7.2$Å^3$/atom showing instability along Γ→N (dotted line) and the spectrum obtained with a harmonic potential modified by the addition of an Einstein model (see text) (solid line). This "pseudo-harmonic" vibrational spectrum allows the calculation of the harmonic contribution to the free energy.

Figure 8: Ab initio free energy of bcc as a f(c/a) at V=7.2 $Å^3$/atom and 5500K. Thermodynamic integration (small λ approximation – Eq. 10) from a mixed reference system (circles); full thermodynamic integration (Eq. 8) over five values for λ between 0 and 1 (squares). Note the possible maximum around c/a = 1 and the minima being approached at c/a < 1 and c/a ~ √2 (fcc).

Figure 9: Stress difference $(\sigma_x + \sigma_{y)/2} - \sigma_z$ as a function of c/a at a zero-strain volume of 7.2 $Å^3$/atom. Open square and open triangles are calculations performed at 5500 K using supercells of 64 and 128 atoms respectively. Filled diamonds are calculations on a 64 atom supercell at 6000K.with a simulation time for each point of ~50-70 ps. The figure suggests that bcc stability increases with temperature.

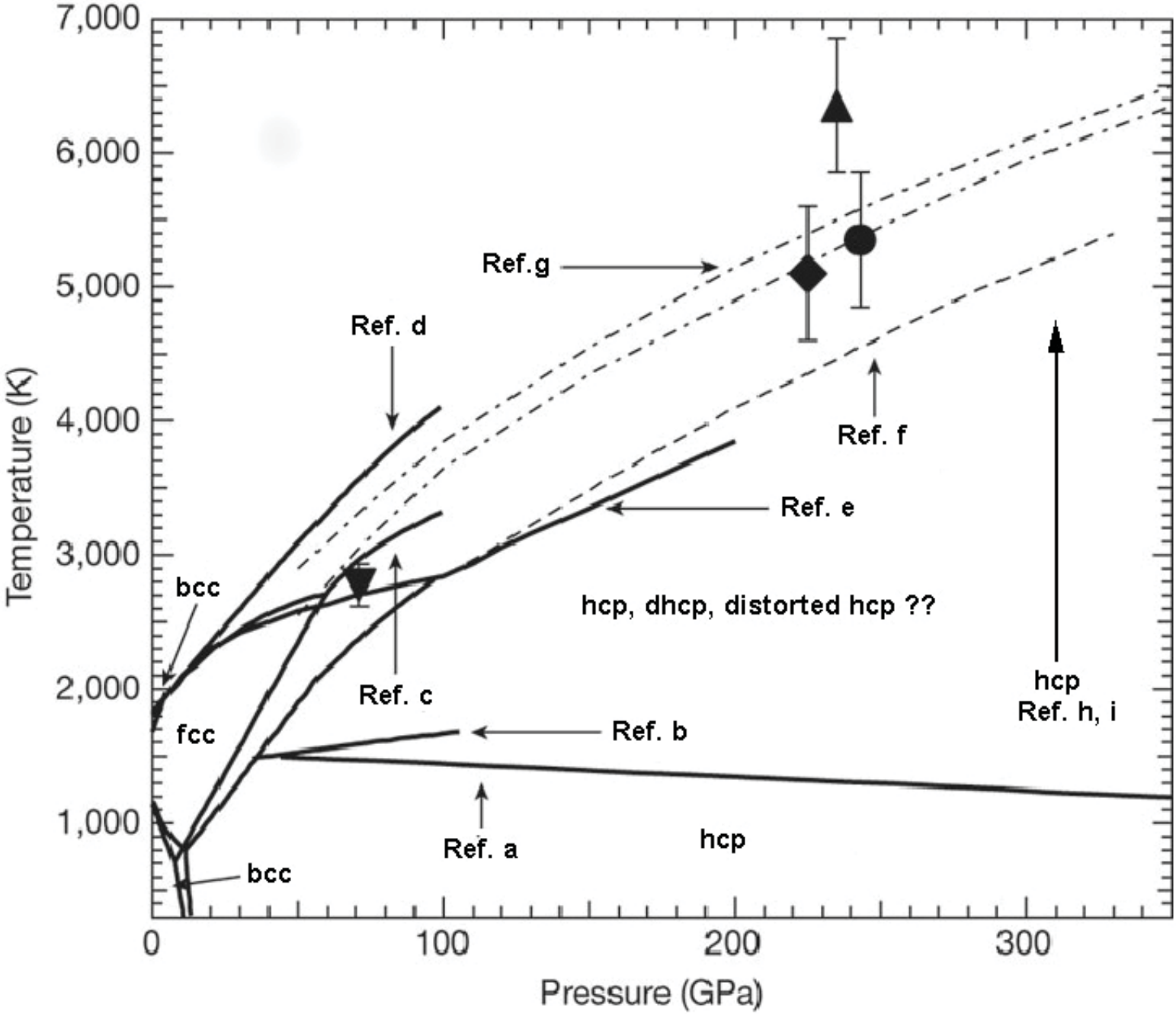
7,000
6,000
5,000
4,000
3,000
2,000
1,000
Temperature (K)
0
100
200
300
Pressure (GPa)
Ref.g
Ref. d
Ref. f
Ref. e
bcc
hcp, dhcp, distorted hcp ??
Ref. c
hcp
Ref. h, i
fcc
Ref. b
Ref. a
hcp
bcc

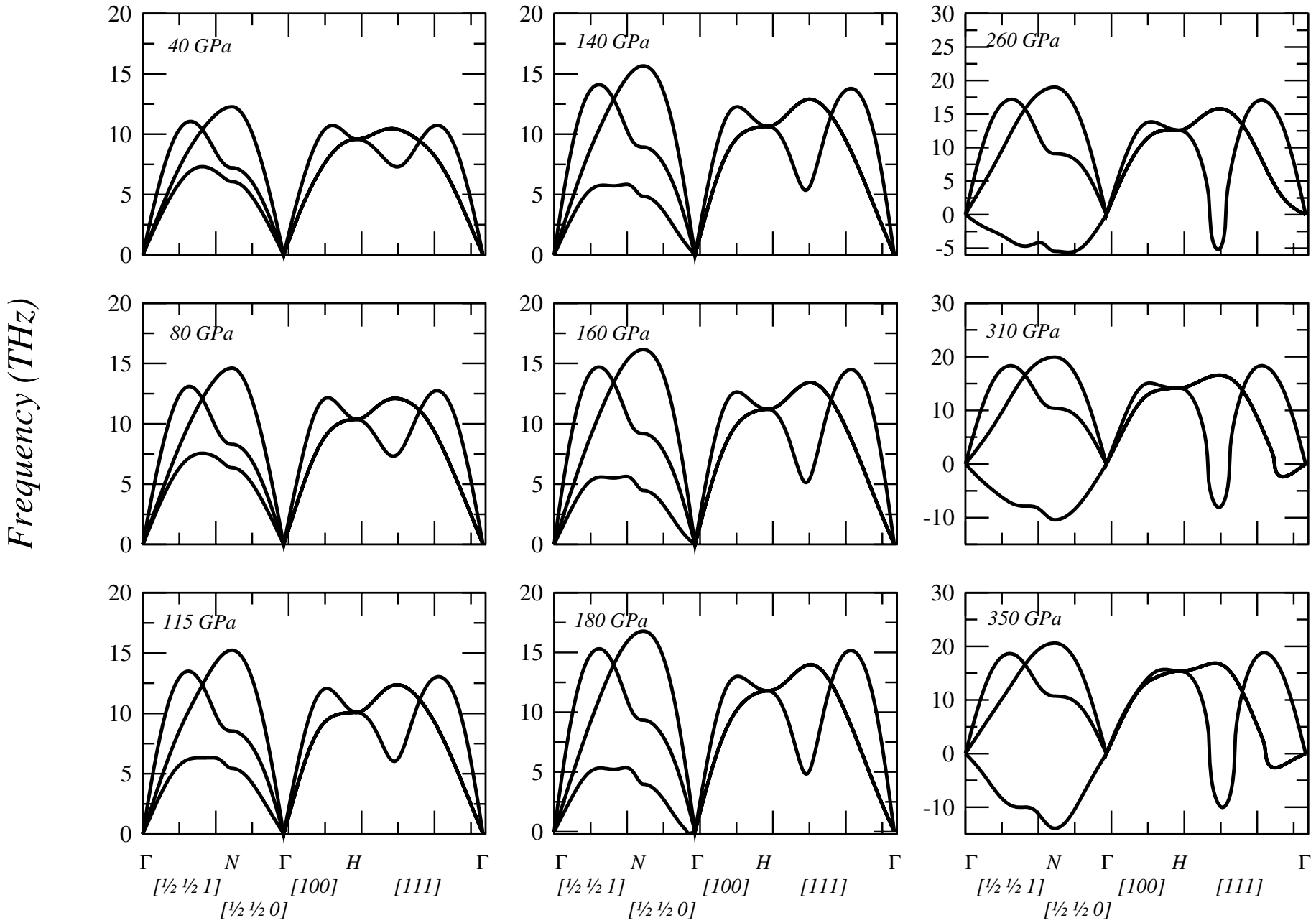
Frequency (THz)
40 GPa
140 GPa
260 GPa
80 GPa
160 GPa
310 GPa
115 GPa
180 GPa
350 GPa
Γ N Γ H Γ
[½ ½ 1] [100] [111]
[½ ½ 0]

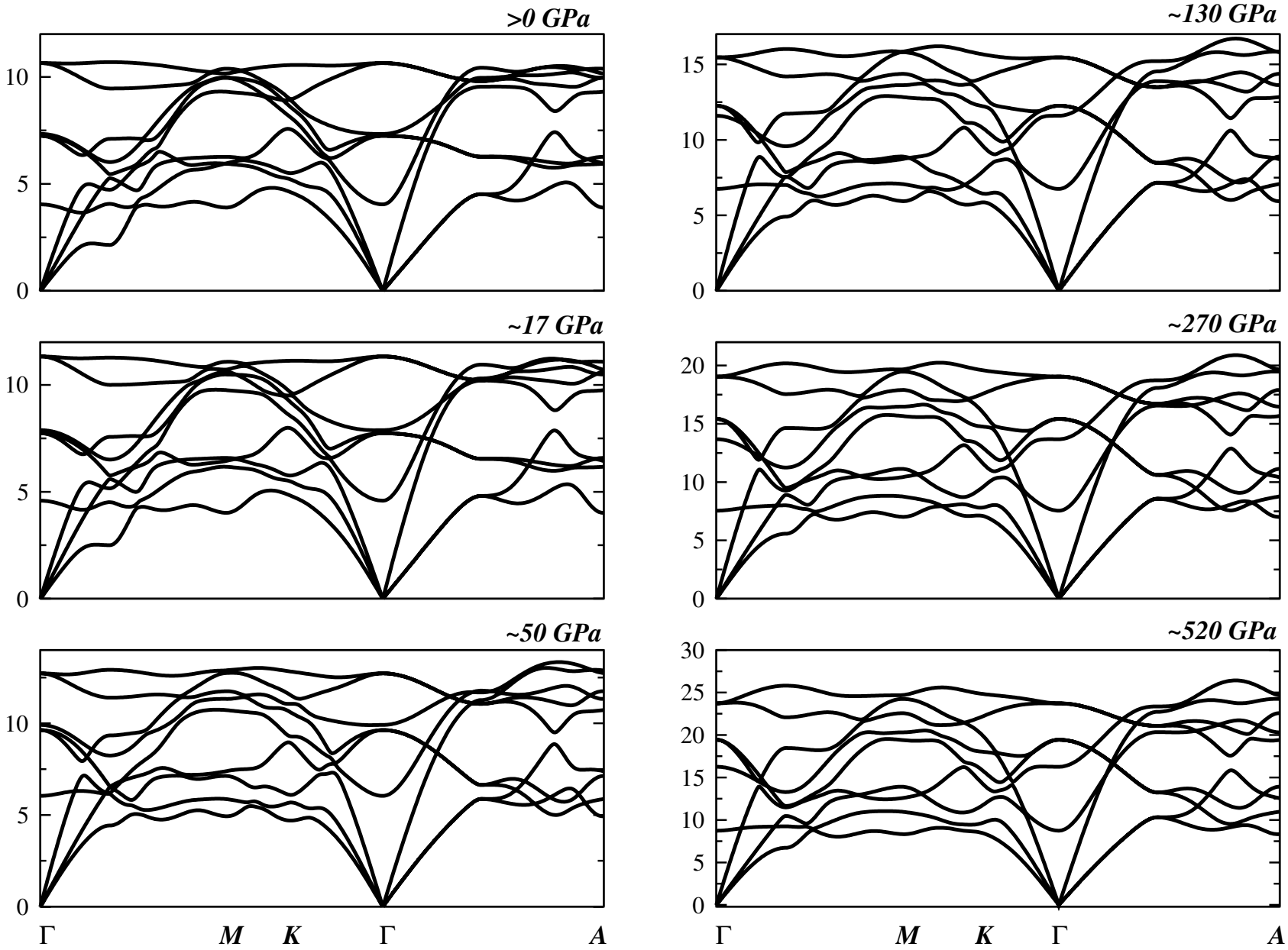
>0 GPa
~130 GPa
~17 GPa
~270 GPa
~50 GPa
~520 GPa
Γ
M
K
Γ
A

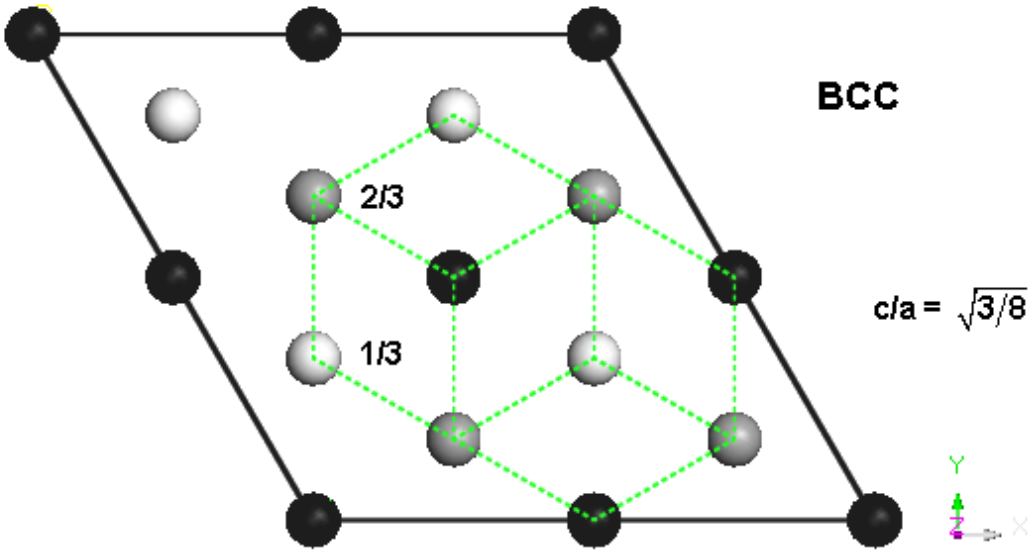
BCC
2/3
1/3
c/a = √3/8
Y
X

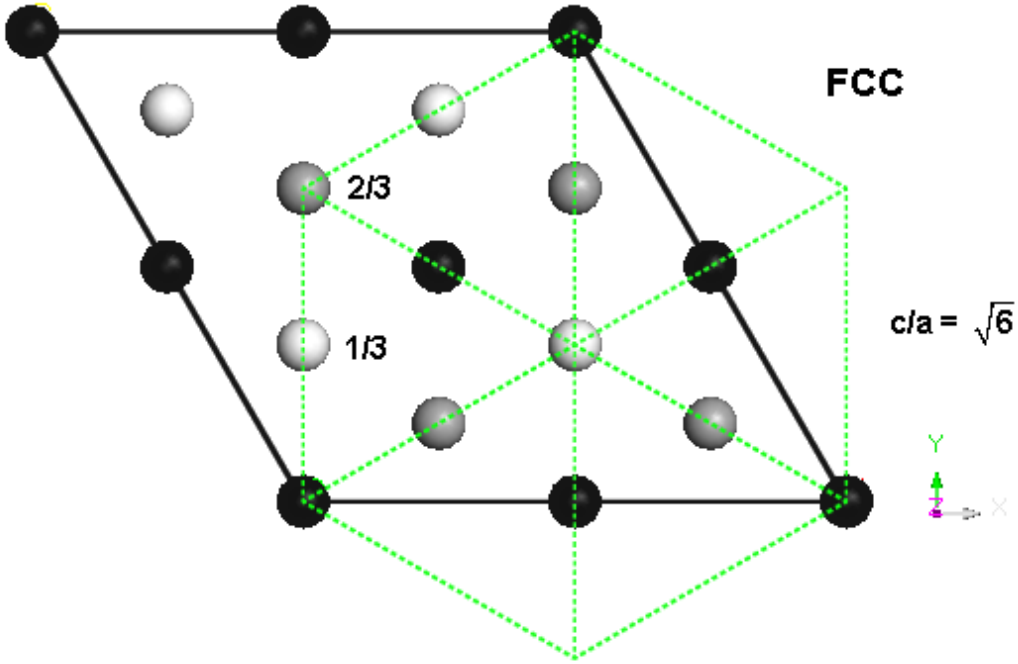
FCC
2/3
1/3
c/a = √6
Y
X

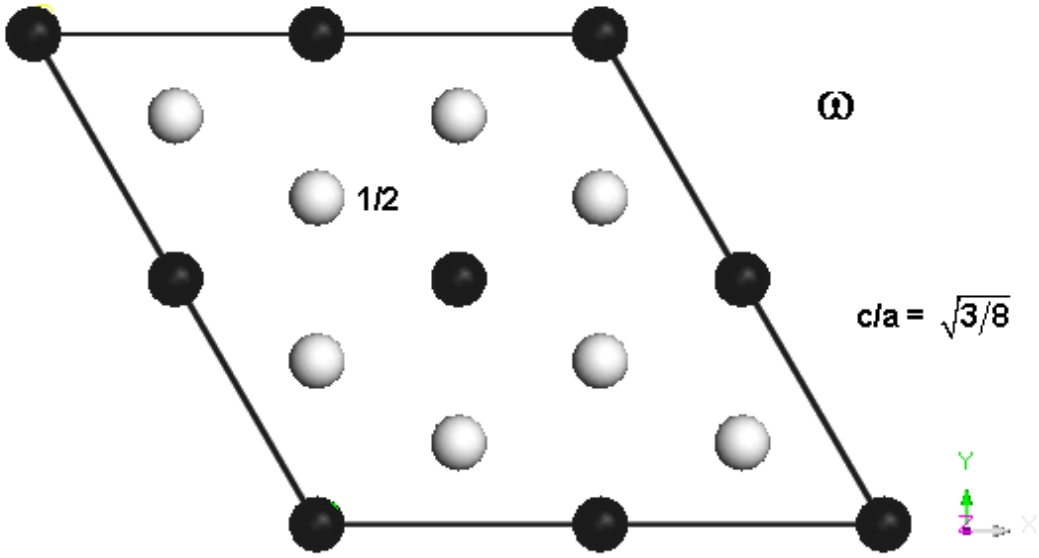
ω
1/2
c/a = √3/8
Y
X

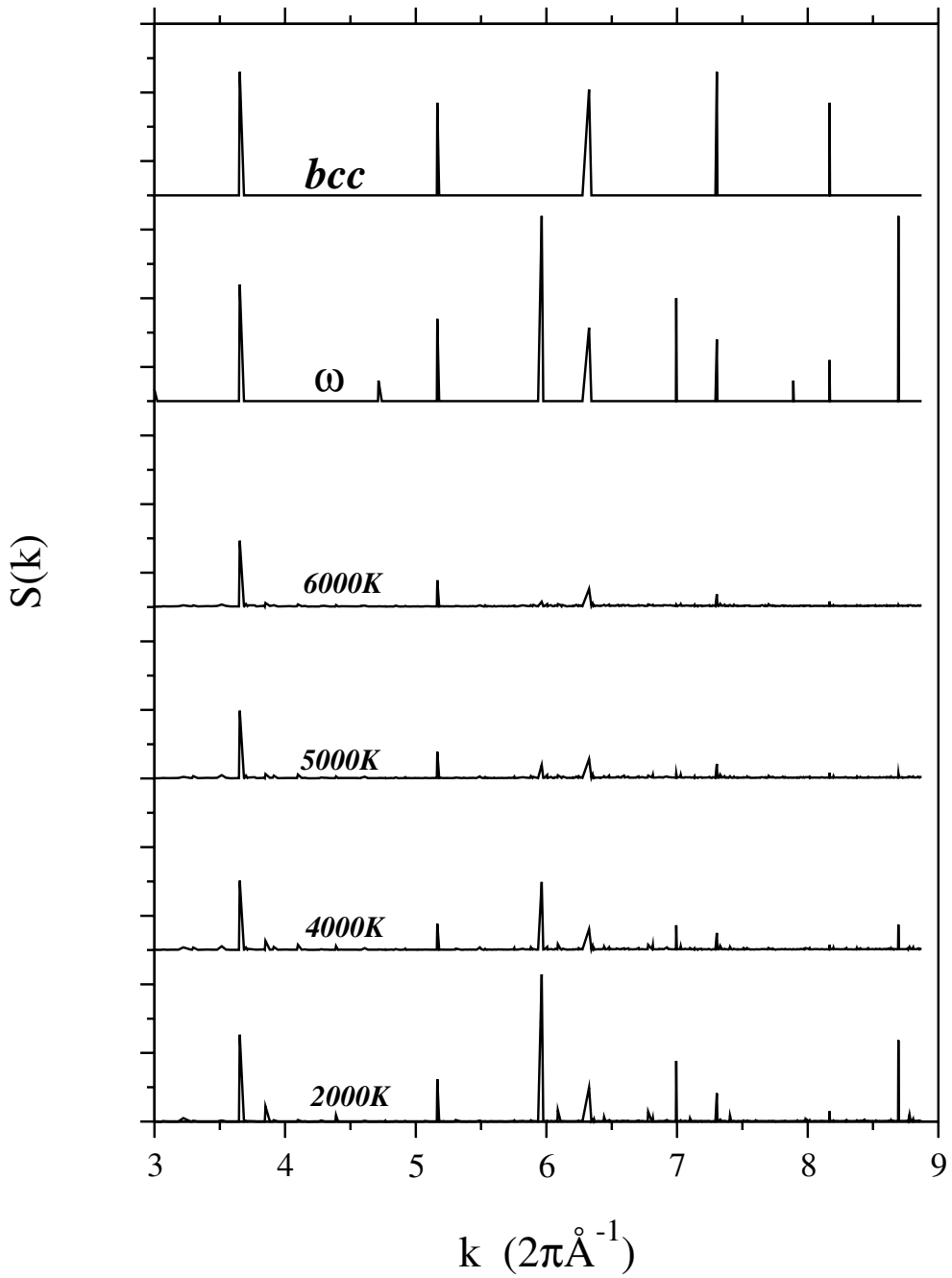
bcc
ω
6000K
5000K
4000K
2000K
S(k)
3
4
5
6
7
8
9
k (2πÅ-1)

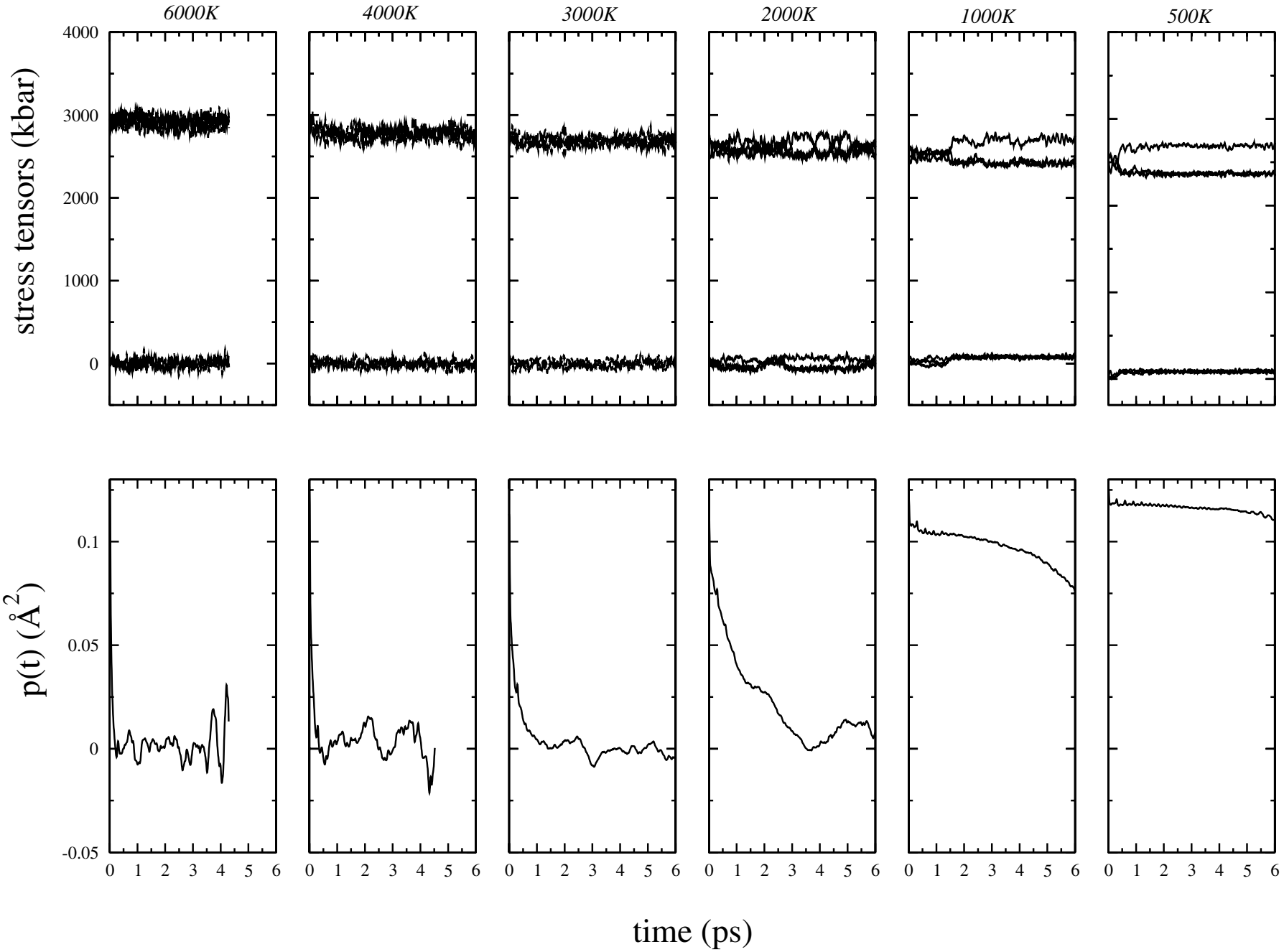
6000K
4000K
3000K
2000K
1000K
500K
stress tensors (kbar)
4000
3000
2000
1000
0
p(t) (Å^2)
0.1
0.05
0
-0.05
0 1 2 3 4 5 6
time (ps)

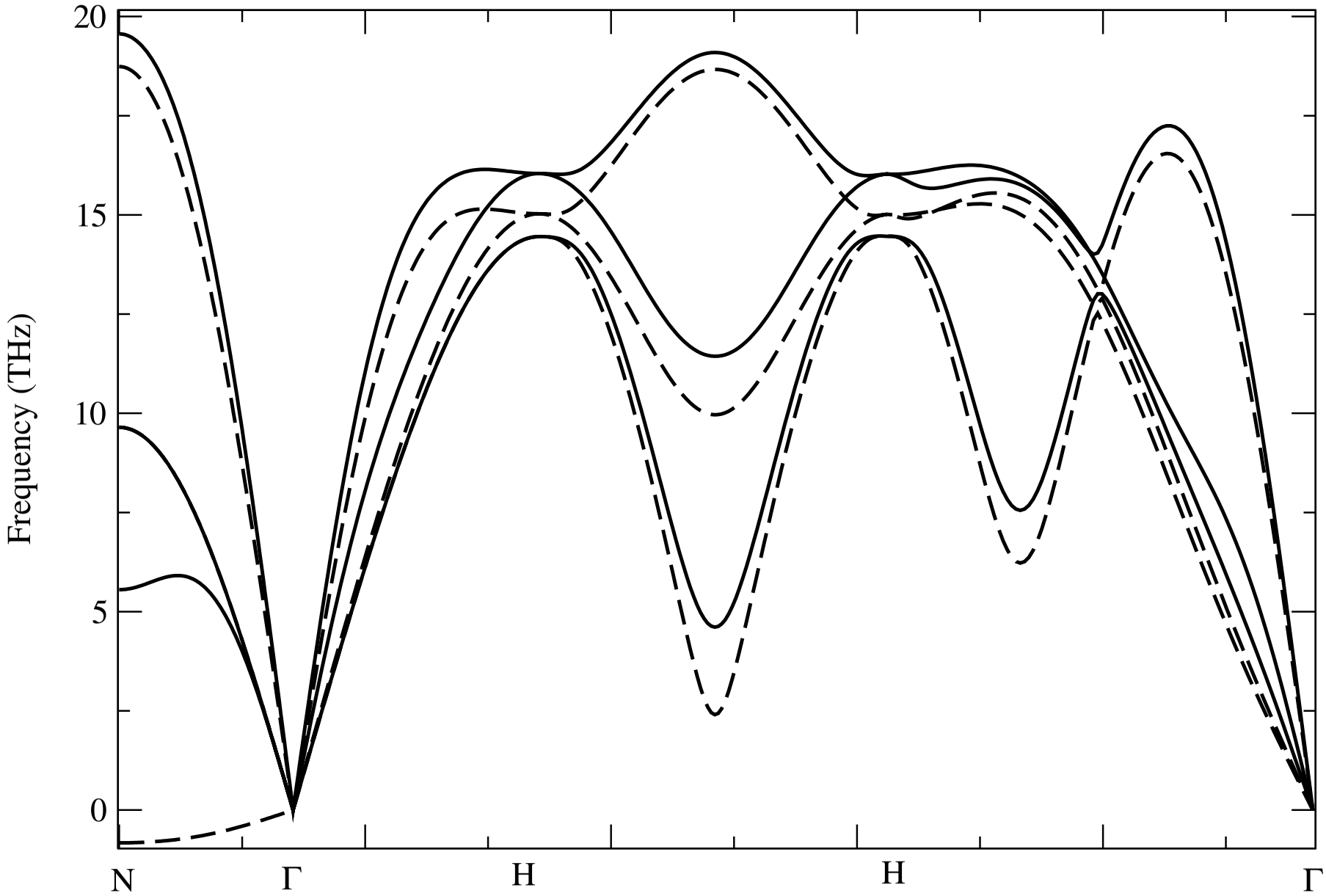
20
15
10
5
0
Frequency (THz)
N
Γ
H
H
Γ

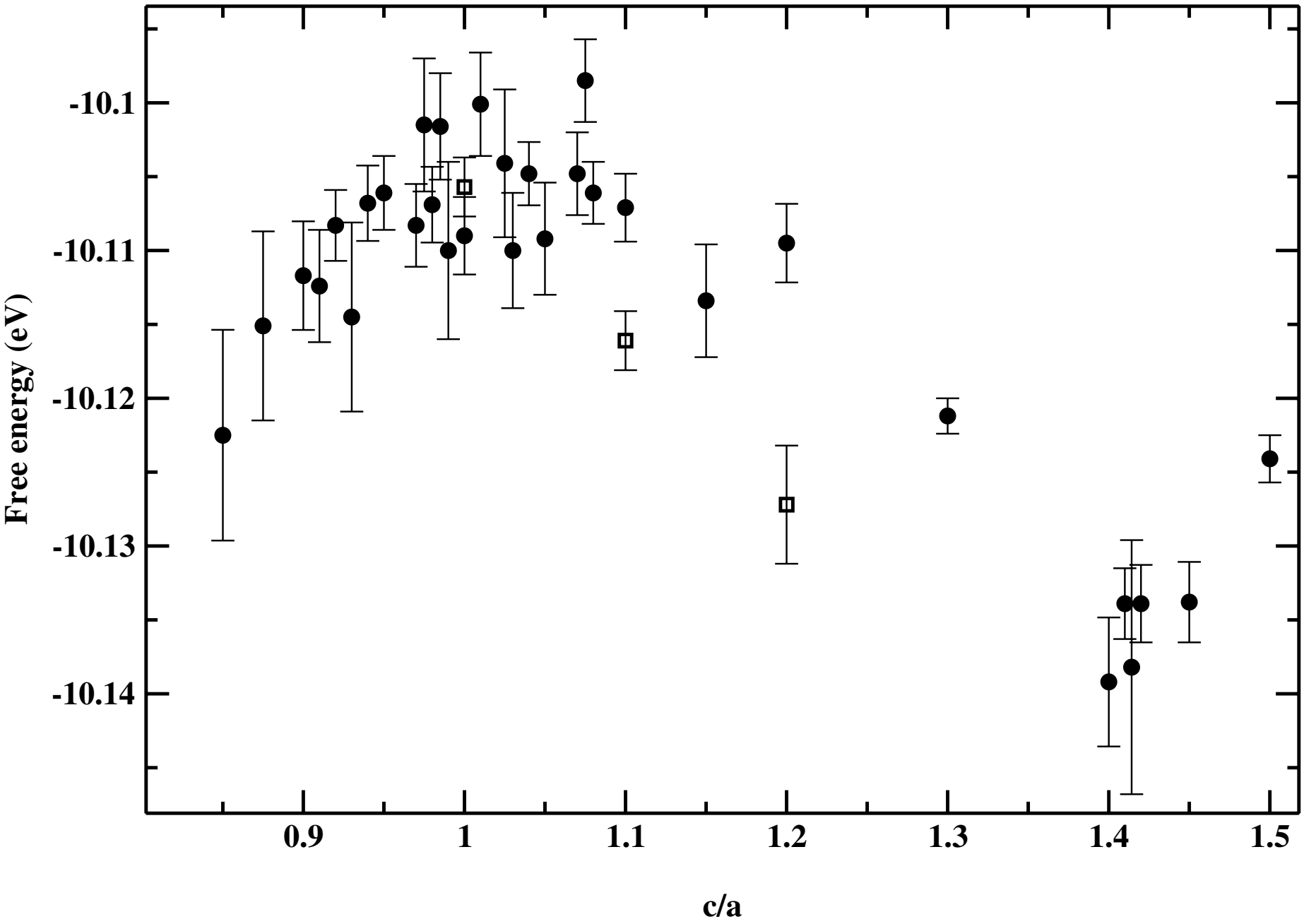
-10.1
-10.11
-10.12
-10.13
-10.14
Free energy (eV)
0.9
1
1.1
1.2
1.3
1.4
1.5
c/a

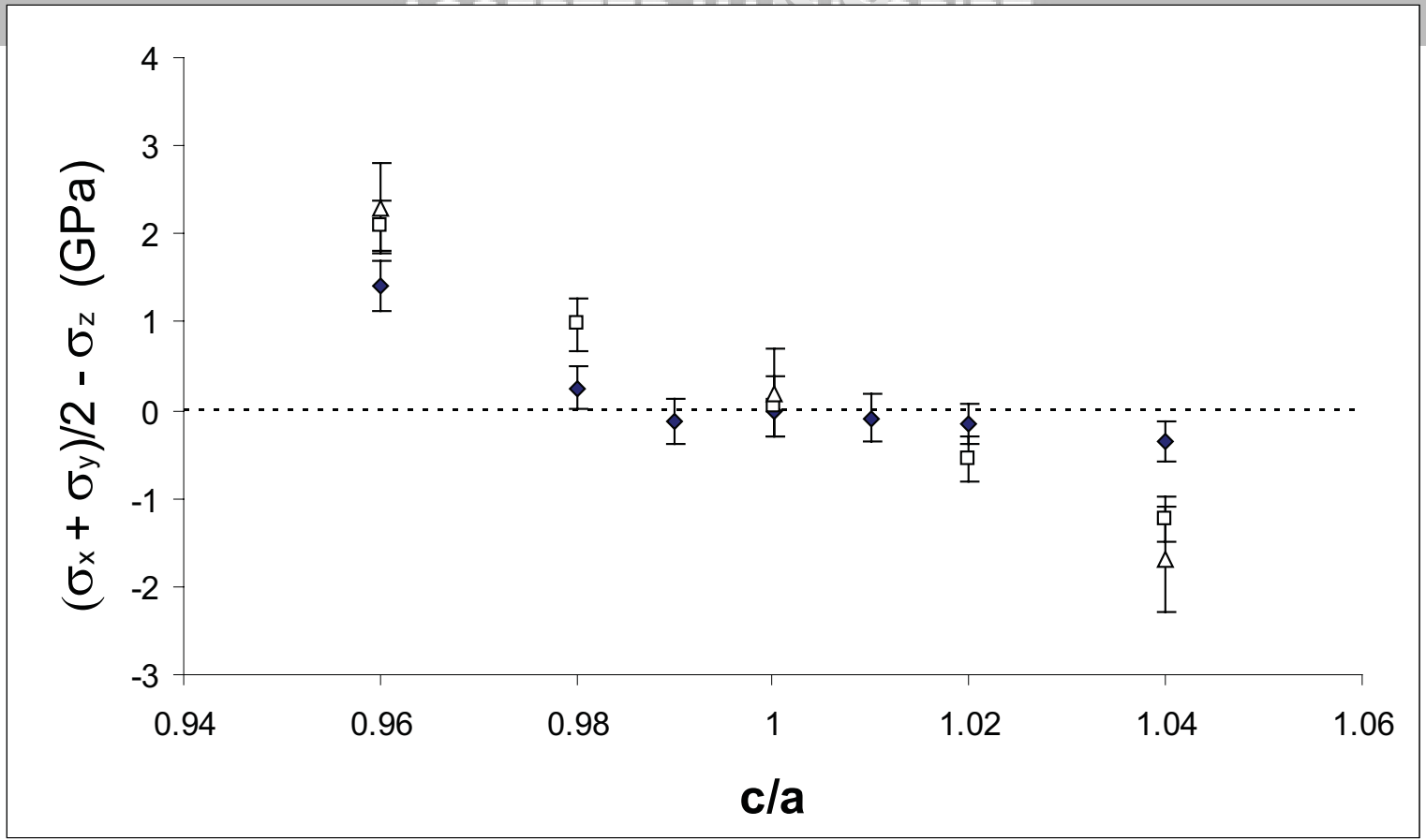
4
3
2
1
0
-1
-2
-3
0.94
0.96
0.98
1
1.02
1.04
1.06
(σx + σy)/2 - σz (GPa)
c/a